1 Introduction

1.1 Technical and Economic Importance of Extruders

Klemens Kohlgrüber

1.1.1 Extruder Types and Terms

Screw machines are used for many process technology tasks. Normally the application takes place in continuous processes in which a screw machine can execute several process tasks simultaneously. It is a "multifunctional" machine. Although screw machines are able to do far more than extrude, mostly the term extruder is used. In the older German use of language also the terms "press" and "kneader" have been used. Corresponding to the old rubber screw presses, screw machines/extruders for plastics have initially been named plastic screw presses. This has been expressed for example by the title "Screw Presses for Plastics" of the first edition of the book of Gerhard Schenkel in 1959. The second edition of 1963 was renamed to "Plastic Extrusion Technology" [1]. Consistent with the current book title "Co-Rotating Twin-Screw Extruders" both terms, screws and extruders, have been "incorporated" into the book at hand.

Werner & Pfleiderer acquired licenses from Bayer for twin-shaft, exactly self-wiping, closely intermeshing co-rotating screw machines (see Section 1.2). They were named "ZSK", and this term was for a long time a synonym for this screw type. The term "ZSK" of Werner & Pfleiderer (today Coperion) is according to the former staff member and author Heinz Herrmann an abbreviation for *Zweiwellige Knetscheibenschneckenpresse* ("twin-shaft screw compounder" in German; [2], p 179). Today the term is mostly shorted to "twin-(shaft)-screw kneader".

For this machine type many synonyms are in use, for example:

- Co-rotating twin screws (tightly intermeshing or non-intermeshing)
- Co-rotating extruder

- Co-rotating, closely intermeshing twin-shaft screw
- Co-rotating twin-screw extruder
- Co-rotating double-screw extruder
- Co-rotating twin-shaft extruder

The closely intermeshing twin-shaft screw with co-rotating shafts occupies a dominant position among the "extruders" and is applied in a variety of processes. An important application is found in the production, compounding, and processing of plastics. The co-rotating screws are also used in other industry sectors, e.g. the rubber and food industry.

1.1.2 Screw Machines and Plastics

The history of the plastics is very short, compared with the history of other materials (e.g., wood, metal, ceramic). The tremendous growth is very clearly illustrated in Figure 1.1.

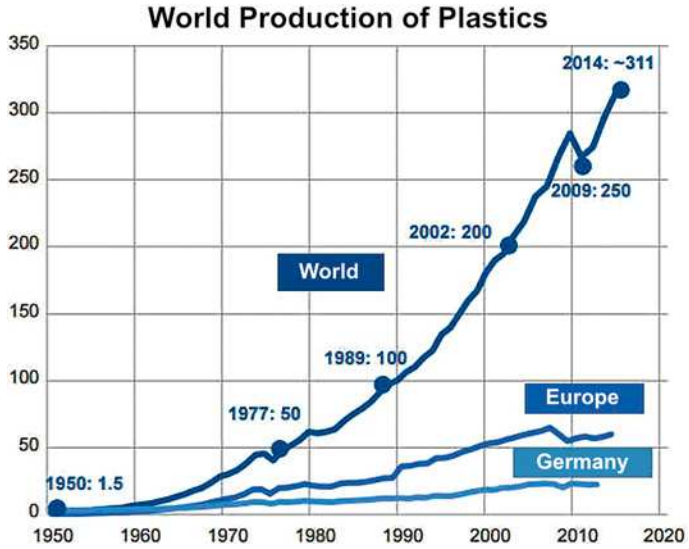

Figure 1.1 Diagram relating to the development of plastics worldwide during the last decades (ordinate: million tons) [Plastics Europe Deutschland e. V.]

What is the connection between the extruder and plastics production?

The success of the plastics industry is closely connected to the success of the extruders. Initially plastics were exclusively compounded discontinuously. This causes, however, economic limits at increasing production quantities. Furthermore, larger quality variations of the material were caused by discontinuous com-

centerline distance. The flanks merge tangentially into the root area. The diameter of the root area corresponds to the diameter of the screw core, and its center is the center of the profile. The tip cleans the root of the opposite screw and vice versa. The corner of the profile between the tip and the flank cleans the opposite flank. This is the basic geometry first described in [3].

2.1.2 The Fully Wiped Profile from Arcs

The basis of closely intermeshing profiles is the fully wiped screw. The individual sections of the profile of the fully wiped screw are arcs. This can be explained on the basis of the kinematic equivalence in which the rotation of the screws is replaced by holding one screw in a fixed position and rotating the other in a circle at a radius equal to the centerline distance.

The first screw (the "generated" screw) is held still in this consideration, and the second screw (the "generating" screw) is moving. After prescribing a part on the generating screw, it is investigated what sort of profile will be generated on the generated screw. In a sense, the generated screw is "cut out" by the generating screw.

First, a point on the generating screw is considered. This point is situated where the tip and the flank merge. This point, together with every other point on the second screw, moves on a circular trajectory with the radius equal to the centerline distance around the first. Examining this line, one obtains the flank; see Figure 2.2.

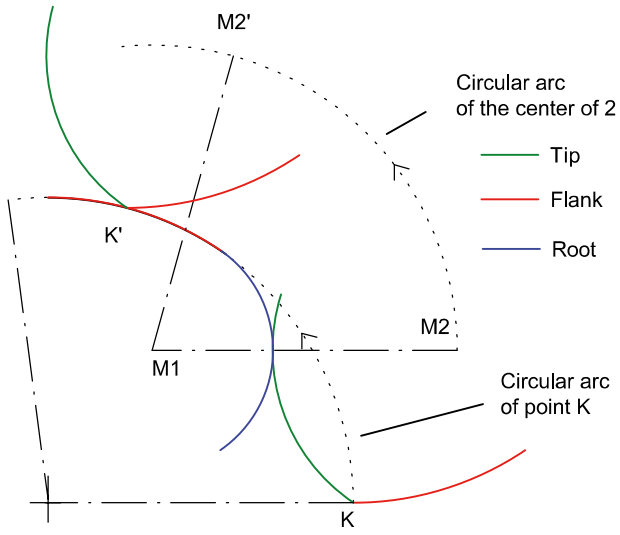

Figure 2.2 Generation of the flank from the transition point between tip and flank of the generating screw

Let us now consider the tip of the generating profile as an arc of radius R. The center of this arc rotates at distance A from the center of the first profile. The contact point between these two profiles, which lies on the root of the generated profile, is always on a line connecting the two centers and is at a distance $RI = A - R$ from the center of the first profile; see Figure 2.3.

Just three variables are required to describe a fully wiped profile (Figure 2.4):

- external diameter DE
- centerline distance A
- number of threads Z

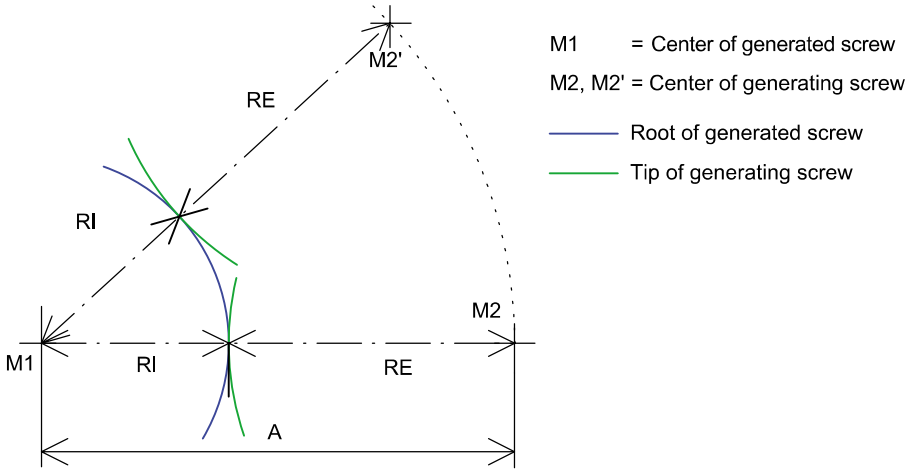

Figure 2.3 Generation of the root as an arc by the tip of the generating screw

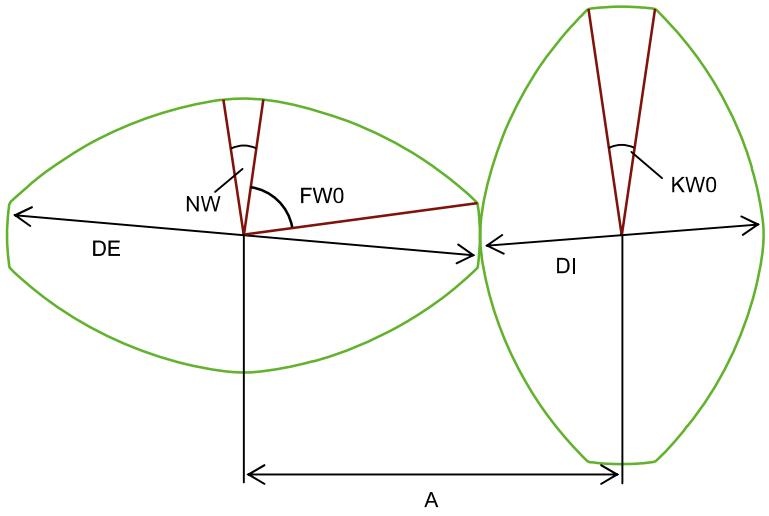

Figure 2.4 Geometric variables of a fully wiped profile

Figure 2.53 Barrier elements

In the case of *eccentric discs* (Figure 2.54) or *one-flighted kneading discs with an integrated extensional channel*, an extensional flow in the peripheral direction occurs. Eccentric discs are cylindrical discs that are arranged eccentrically to the screw shaft. The product is drawn into the tapering eccentric gap by the rotational movement of the discs and is thus extended. However, the flow is not led in the axial direction so that parts of the product can deviate up- and downstream and particles are not subject to any defined extension.

Figure 2.54 Eccentric discs

Figure 2.55 Single-flighted kneading discs with extension channel

In one-flighted kneading discs, the eccentric disc is contained on both sides by a one-flighted profile disc. The polymer that is drawn into the extension channel can no longer escape to the sides and thus is subject to the full extension flow as defined by the geometry.

In similar fashion to the kneading discs, both disc implementations can be combined into larger element units.

In the *screw shear elements* (Figure 2.56), shear gaps are worked into the screw crest section by section. In these gaps, a portion of the melt is exposed to a defined shear field in order to disperse higher molecular polymer content, for example. One should bear in mind with these elements that the stress of the material does not occur quantitatively across the entire product stream.

Figure 2.56 Screw shear elements

2.3.1 WO 2009152910, EP 2291277, US 20110110183

Filing date: 2008-06-20

Company: Bayer Technology Services, now Covestro

This patent shows universally how one- to four-flight, self-cleaning screw profiles can be constructed from circular arcs using symmetries. Furthermore, the patent discusses how complete, self-cleaning screw profiles can be created from circular arcs using a transition element as an example.

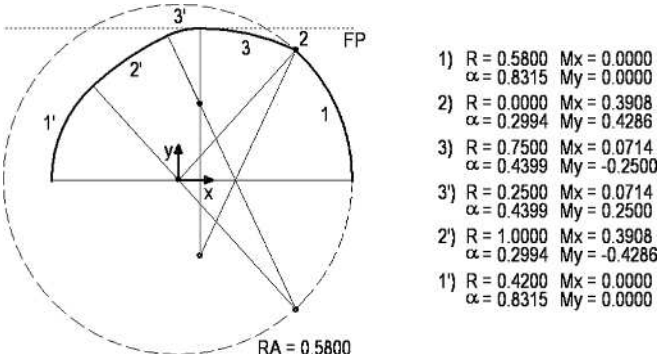

Figure 2.59

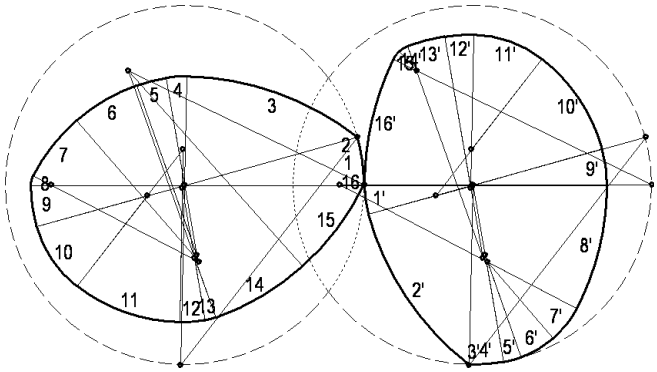

Figure 2.60

2.3.2 WO 2011039016, EP 2483051, US 20120320702

Filing date: 2009-09-29

Company: Coperion, formerly Werner & Pfleiderer

In this patent, the section of a screw profile is obtained over an evolute E, which consists of a set of points P(1) to P(*n*). The involute of a point-shaped evolute is a circle (arc), so that in the end, the design rule shown is also based on circular arcs.

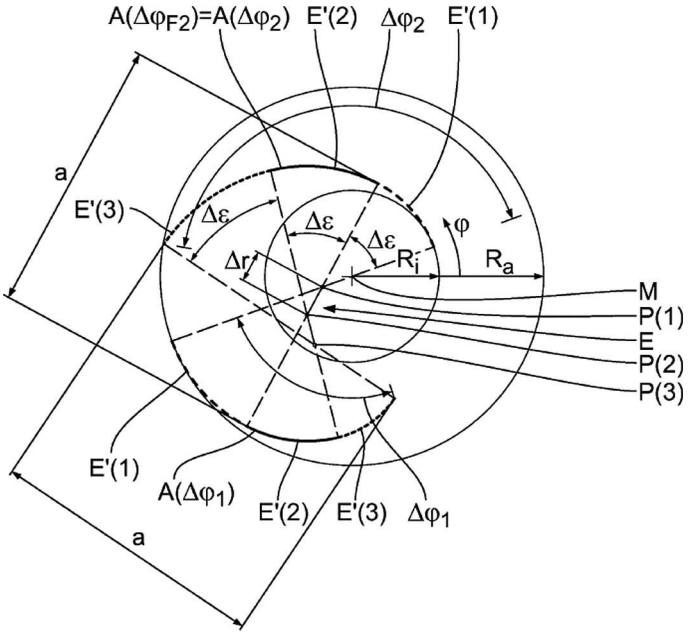

Figure 2.61

Figure 3.2 illustrates a classification of the rheological behavior of solids and fluids. Examples of different flow behaviors are shown in the lowest boxes. Figure 3.2 also illustrates the resulting shear stress as a function of the (shear) deformation γ or, for fluids, the shear rate $\dot{\gamma}$. The two most important material properties for our discussion in this chapter are the viscoelastic and the Newtonian fluid circled in the figure.

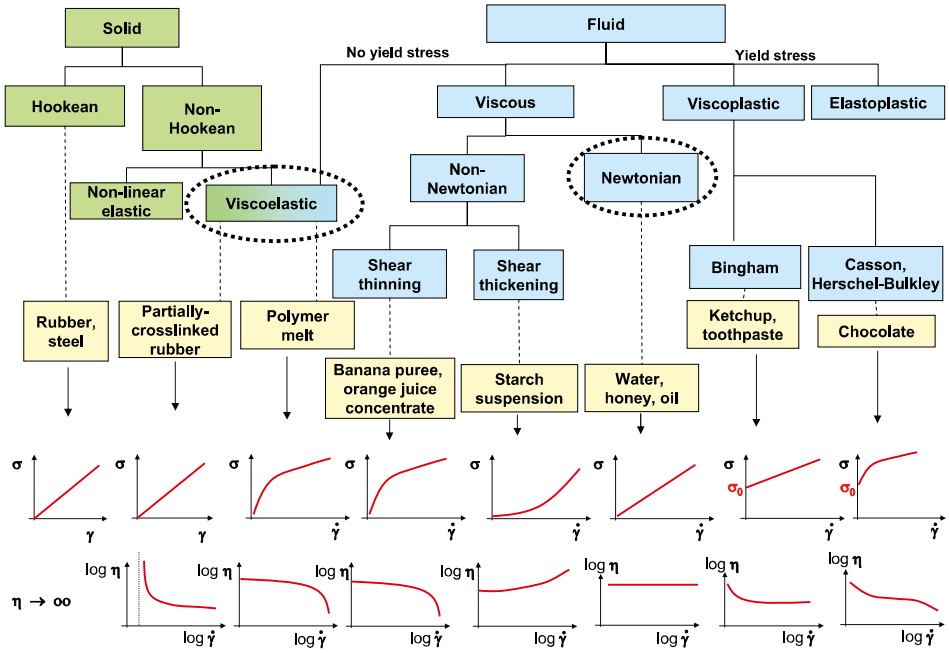

Figure 3.2 Different types of rheological behavior of solids and fluids with examples of materials [7]. Bottom: shear stress as a function of the deformation γ or shear rate $\dot{\gamma}$ and shear viscosity η as a function of the shear rate $\dot{\gamma}$ (double-logarithmic axes)

In the case of solids it is evident that deformation is either linear elastic – like a Hookean solid (most solids including steel and rubber) – or non-linear elastic or viscoelastic. In the case of liquids, fluids differ between those without yield stress and those with yield stress (so-called plastic materials). Fluids without yield stress will flow if subjected to even slight shear stresses, while fluids with yield stress start to flow only above a material-specific shear stress which is indicated by σ_0.

In the case of fluids *without* yield stress, viscous and viscoelastic fluids can be distinguished. The properties of viscoelastic fluids lie between those of elastic solids and those of Newtonian fluids. There are some viscous fluids whose viscosity does not change in relation to the stress (Newtonian fluids) and some whose shear viscosity η depends on the shear rate $\dot{\gamma}$ (non-Newtonian fluids). If the viscosity

increases when a deformation is imposed, we define the material as a shear-thickening (dilatant) fluid. If viscosity decreases, we define it as a shear-thinning fluid.

In the case of fluids *with* yield stress, viscoplastic fluids differ from elastoplastic fluids. With the application of a shear stress σ above the yield strength σ_0, Bingham fluids show a linear dependence of shear stress on shear rate, whereas Casson and Herschel-Bulkley fluids show a nonlinear dependence on these parameters.

Newtonian fluids display the simplest rheological behavior. They show a constant viscosity η and there is a direct proportionality between the shear rate $\dot{\gamma}$ and shear stress σ:

$$\sigma = \eta \cdot \dot{\gamma} \tag{3.4}$$

Non-Newtonian fluids whose viscosity depends on shear rate can be described using a power law:

$$\sigma = K \cdot (\dot{\gamma})^n \tag{3.5}$$

Equation (3.5) contains a constant factor K and a varying factor n, which specifies the slope of the of the viscosity function. For Newtonian fluids, K corresponds to the shear viscosity η and $n = 1$. For $0 < n < 1$, the fluid is a shear thinning fluid. For shear-thickening fluids, i.e. liquids, whose viscosity increases with shearing, $1 < n < \infty$.

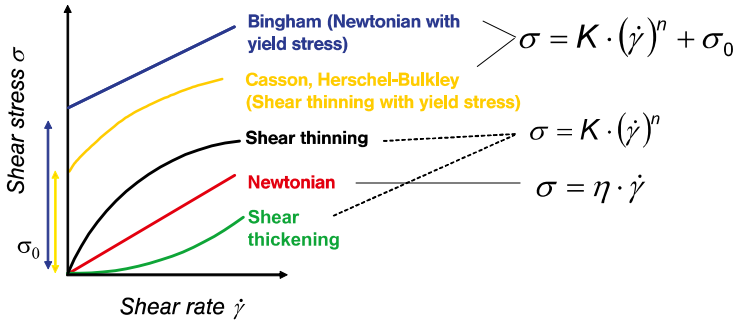

Figure 3.3 Graphical illustration of Equation (3.6)

Figure 3.2 and Figure 3.3 show the sub-division of fluids into those with and without yield stress. Fluids with yield stress require a shear stress σ_0 in order to flow. We are all familiar with this characteristic from tomato ketchup, which requires a certain "minimum force" before it starts to flow out of the bottle. Below σ_0 it is still a solid – in rheological terms. This behavior is described in the model by adding a shear stress σ_0 to Equation (3.5). We then obtain a Herschel-Bulkley correlation:

Instantaneous and Average Mass Flow Rates

For the design of machines like extruders or other devices for sorption processes the knowledge of the concentration profiles at the phase boundary alone is not sufficient. However, it forms the basis to derive relationships to estimate the mass fluxes caused by diffusion between the phases. Suitable reference values for the dimensionless representation of mass flow rates result from the individual application. For this reason, the results for instantaneous and average mass flow rates are not presented here in dimensionless groups. Only the relationships for the mean liquid concentration are presented again as a dimensionless group.

From Equation (3.26) for the local concentration gradient at the phase boundary at $x = 0$ the following relationship results:

$$\left.\frac{\partial \rho_j}{\partial x}\right|_{x=0} = \left(\rho_{j,0} - \rho_{j,gl}\right)\frac{1}{\sqrt{\pi D_f t}} \tag{3.42}$$

With this expression and Fick's first law, Equation (3.26), it follows for the mass flux diffusing from the liquid element at the phase boundary into the gas phase $\dot{m}_j$:

$$\dot{m}_j = -\frac{1}{\sqrt{\pi}}\left(\rho_{j,0} - \rho_{j,gl}\right)\left(\frac{D_f}{t}\right)^{1/2} \tag{3.43}$$

The relationship given by Equation (3.43) describes the diffusive mass transport on the liquid side of the phase interface. Both the proportionality $\dot{m}_j \sim \left(\rho_{j,0} - \rho_{j,gl}\right)$ as well as $\dot{m}_j \sim \sqrt{D_f / t}$ are typical of this kind of molecular mass transport.

For many practical tasks, instead of the instantaneous value of the mass flux $\dot{m}_j$ information about the time average value $\dot{\bar{m}}_j$ in the time interval $t_0 \le t \le t_E$ is required. With the mathematical definition of the time average value and Equation (3.43) for $\dot{m}_j$ it follows:

$$\dot{\bar{m}}_j \equiv \frac{1}{\left(t_E - t_0\right)}\int_{t_0}^{t_E} \dot{m}_j dt = -\frac{2}{\sqrt{\pi}}\left(\rho_{j,0} - \rho_{j,gl}\right) D_f^{1/2}\frac{\left(t_E^{1/2} - t_0^{1/2}\right)}{\left(t_E - t_0\right)} \tag{3.44}$$

With this relation the time average of the mass flux $\dot{\bar{m}}_j$ for any time interval $t_0 \le t \le t_E$ can be calculated. With regard to the limit

$$\lim_{t_0 \to t_E}\left(\frac{t_E^{1/2} - t_0^{1/2}}{t_E - t_0}\right) = \frac{1}{2t^{1/2}} \tag{3.45}$$

for $t_0 \to t_E$ then $\dot{\bar{m}}_j = \dot{m}_j$ applies, as shown in the comparison of Equation (3.44) with Equation (3.43).

For the time interval $0 \le t \le t_E$ the relationship is simplified because of $t_0 = 0$:

$$\dot{\bar{m}}_j = -\frac{2}{\sqrt{\pi}}\left(\rho_{j,0} - \rho_{j,gl}\right)\left(\frac{D_f}{t_E}\right)^{1/2} \tag{3.46}$$

The time average value $\dot{\bar{m}}_j$ for the interval $0 \le t \le t_E$ differs in this case from the instantaneous value $\dot{m}_j$ at time $t = t_E$ by a factor of 2.

By integration of the mass flux $\dot{m}_j$ or $\dot{\bar{m}}_j$ over the phase interface S the instantaneous and average mass flows diffusing over the phase interface are obtained. For the average mass flow $\dot{\bar{M}}_j$ in the time interval $0 \le t \le t_E$ it follows:

$$\dot{\bar{M}}_j = -\frac{2}{\sqrt{\pi}}\left(\rho_{j,0} - \rho_{j,gl}\right) D_f^{1/2} \iint t_E^{-1/2} dS \tag{3.47}$$

The integral expression considers that the phase interface S can vary with time and that different values are possible for the time interval $0 \le t \le t_E$ in which a liquid element is present at the phase interface.

Multiplying the average mass flow $\dot{\bar{M}}_j$ with time t_E gives the mass $\Delta\bar{M}_j$ exchanged by diffusion between the phases in the time interval $0 \le t \le t_E$:

$$\Delta\bar{M}_j = \dot{\bar{M}}_j t_E = -\frac{2}{\sqrt{\pi}}\left(\rho_{j,0} - \rho_{j,gl}\right) D_f^{1/2} \iint t_E^{1/2} dS \tag{3.48}$$

Equations (3.47) and (3.48) indirectly represent the basic relationship between diffusive mass transport over a phase interface and the relevant parameters of the liquid system, the operating conditions, and the geometry. The direct dependency can only be derived from the specific application by determining the individual values for liquid properties, operating conditions, and geometry for each of the variables on the right side of Equations (3.47) and (3.48).

With the relationships reported here for the instantaneous and average mass flow rates, it is common practice in process engineering to define mass transfer coefficients. This historically caused procedure is also used to describe the mass transport in screw machines [8–10]. However, it does not provide any additional information in the theoretically deduced relationships for mass transport, but it requires additional calculation effort in the application [1]. Therefore, no mass transfer coefficients are introduced here but direct relationships to determine the mean concentration of the volatile species in the polymer melt are derived from the mass balance.

Table 3.12 Material: PS; Wedge Gap Opening Angle: $\alpha = 40°$

v_h in mm s^{-1}	$\gamma_{yxtoth2}$	γ_{toth2}	e_{xtoth2}	ε_{xtoth2}	$\dot{\varepsilon}_{xm}$ in s^{-1}	$\sigma \cdot 10^5$ in Pa
1200	6.5	982.8	56.6	4.0	366	2.4
2400	6.6	1238.6	67.7	4.2	764	2.8
3600	6.6	1411.2	74.7	4.3	1173	3.1

In the six tables it can be seen that the total shear deformation $\gamma_{yxtoth2}$ at a given wedge gap geometry is independent of the moving plate speed v_h and the mean total deformation γ_{toth2} increases with the mean planar stretching e_{xtoth2} in all plastic melts. The achievable mean Hencky strain ε_{xtoth2} is high for the more viscous and more pronounced pseudoplastic melts. The strain induced deformation for each individual drop of the melt lies at a very high level. The high mean strain rates are increased with increasing moving plate speed v_h. The mean tensile stress reaches values of $\sigma = 10^6$ Pa for the highly viscous PE-HD melt. This was measured by Hürlimann [11] with a capillary rheometer. At the capillary exit melt fracture was observed. Bernnat [9] verified with in rheotens experiments comparable critical tensile stresses. Also at lower strain levels drop breakage is possible on a large number of melt drops when they are exposed to much higher local tensile stresses in the wedge gap. In general one can find that for more pronounced pseudoplastic flow behavior of the melt the wedge gap geometries with a large opening angle α are more effective. Furthermore, the increase in total shear deformation can be adjusted over the flat gap length. The total mean elongation, the mean strain rate, and the mean tensile stress are adjustable over the moving plate speed v_h.

3.5.1.4.5 Deborah Number Depending on the Moving Plate Speed

The Deborah number *De* (Equation (3.99)) was calculated for the six plastic melts in the wedge gap ($l_e = 0$ mm) for two moving plate speeds. The results are summarized in Tables 3.13 and 3.14.

Table 3.13 Deborah Number De for Six Plastic Melts in the Wedge Gap with the Moving Plate Speed $v_h = 1200$ mm s^{-1}, $\alpha = 15°$, $l_k = 4$ mm

Material	PC	PA 6	PE-HD	PE-LLD	PP	PS
t_K in ms	7.9	7.8	7.7	7.7	7.6	7.6
De	0.16	0.13	285	4.1	16.4	77.5

Table 3.14 Deborah Number De for Six Plastic Melts in the Wedge Gap with the Moving Plate Speed $v_h = 3600\ \text{mm s}^{-1}$, $\alpha = 15°$, $l_K = 4\ \text{mm}$

Material	PC	PA 6	PE-HD	PE-LLD	PP	PS
t_K in ms	2.6	2.6	2.6	2.6	2.5	2.5
De	0.49	0.38	858	12.4	49.2	232

Already at the moving plate speed $v_h = 1200\ \text{mm s}^{-1}$ the Deborah numbers are significantly larger than 1 for the more pronounced entropy-elastic melts (with higher *B*-value of the Carreau approach, Equation (3.88)), so the viscoelastic melt drops show more the deformation behavior of a solid body. That means drop breakage due to the viscoelastic properties of the melt is favored when the characteristic relaxation time is sufficient large and the residence time of the melt in the wedge gap is sufficiently short (i. e., short wedge gap length with a few millimeters l_K and large wedge gap angle α). At lower disc speeds the Deborah numbers are smaller and the tensile stresses obtained are too low for a drop size reduction.

3.5.1.4.6 Local and Average Dissipative Temperature Increase in the Wedge Gap/Flat Gap System

The temperature increase in the melt by shear, planar elongation, and resulting total deformation at the exit of the wedge gap/flat gap system are plotted over the *y*-coordinate in Figure 3.61. The temperature of the melt rises very sharply on the fixed wall. The dispersive shear element can heat up and the dispersive mixing effect can be reduced. Therefore the geometry and the circumferential speed of the shear element must be adjusted due to the flow behavior and the thermal properties of the melt.

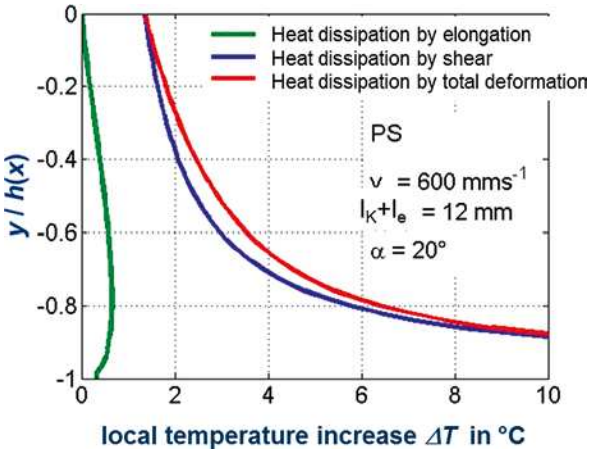

Figure 3.61 Local temperature increase for a PS melt at the wedge gap/flat gap exit

screw tips. Figure 4.80 shows the temperatures directly on the screw surfaces. The color scale in the two illustrations ranges from 300 °C (blue) to 350 °C (red). In addition, Figure 4.81 shows a diagram which displays the maximum temperature on the screw tip over the rotation of the conveying element.

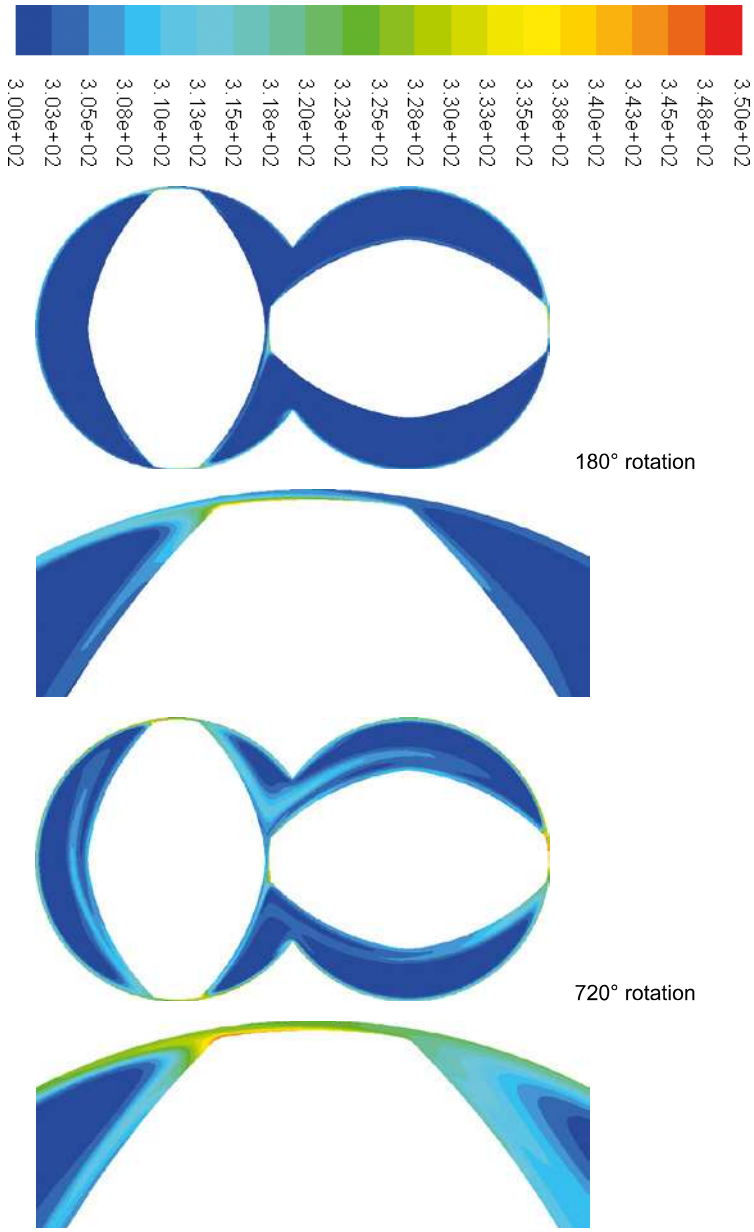

Figure 4.79 Temperature of the polymer melt in the cross-section of a conveying element with adiabatic walls after a half turn and after two turns, each with a detailed enlargement around one of the screw tips

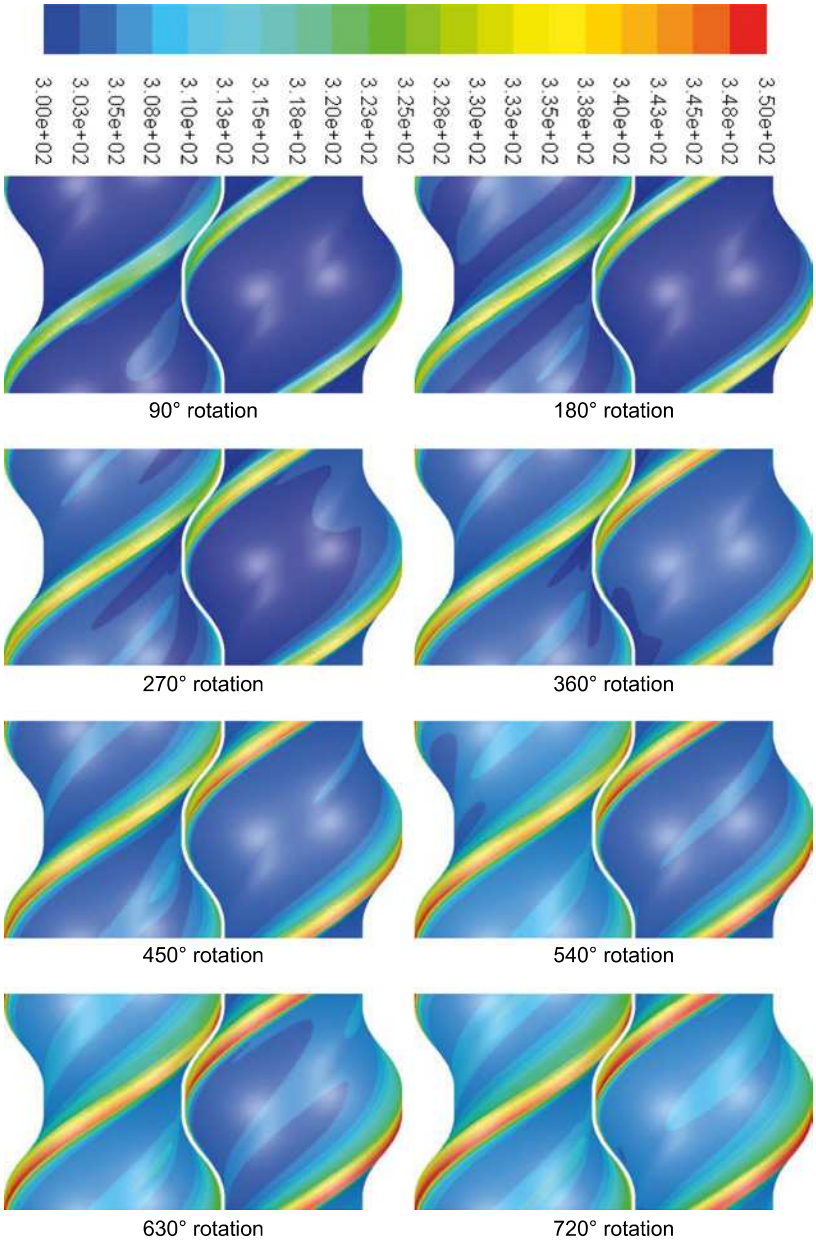

Figure 4.80 Temperature of the polymer melt on the screw surface of a conveying element within two revolutions

Since most of the heat is generated directly in the vicinity of the screw tips, the temperature initially rises to 339 °C within half a revolution. Afterwards, a significantly slower temperature rise can be observed on the surface of the screw tip. This is due to the fact that the heated fluid continuously leaves the tip area and